PHYSICAL REVIEW D **81,** 024008 (2010)

Nonequatorial charged particle confinement around Kerr black holes

Giovanni Preti*

Dipartimento di Fisica "Galileo Galilei," Università degli Studi di Padova, and INFN Sezione di Padova, 35131 Padova, Italy

(Received 24 June 2009; published 13 January 2010)

We analyze the nonequatorial charged particle dynamics around a rotating black hole in the presence of an external magnetic field, the latter being given by Wald's exact analytical solution to the Maxwell's equations in the Kerr background. At variance with the corresponding Schwarzschild case, the behavior of the particle becomes here markedly charge-sign dependent, and the more so the more the Kerr parameter increases. The interplay between the rotating black hole and the magnetic field is shown to provide a mechanism both for selective charge ejection in axially collimated jetlike trajectories, and for selective charge confinement into nonequatorial bound orbits around the hole; the possibility of such a confinement allows the fate of an accreting particle to not necessarily be doomed: infall into the hole can be prevented, and the neutrality of the Kerr source could therefore be preserved, while the charge is safely parked into bound cross-equatorial orbits all around it.

DOI: 10.1103/PhysRevD.81.024008 PACS numbers: 04.20.−q, 04.70.Bw

I. INTRODUCTION

A remarkable characteristic of the spacetimes of the Kerr family is their allowing separation of the geodesic Hamilton-Jacobi equation into a radial and an angular part, when the metric is written in oblate spheroidal ("Boyer-Lindquist") coordinates [1]. The nontrivial existence of a fourth constant of motion, which is related to the existence of a Stäckel-Killing tensor [2–5], and the physical meaning of which has been illustrated in [6], allows reduction of the geodesic problem to quadratures. This fact obviously provides a notable simplification for both analytical and numerical calculations; in particular, it allows a complete characterization of the equatorial orbits, which are of primary importance for astrophysical applications, e.g. in relation to accretion disks. Nonequatorial motions are certainly not less important, though, and astrophysically interesting as well, with applications, e.g., to the jet phenomena and the sheaths of ionized matter enveloping the accretion centers; these nonequatorial motions therefore deserve due attention as well. In the nonequatorial case, yet, the analysis becomes more complex, since it requires investigation of three-dimensional spatial structures instead of the simpler planar ones. Moreover, complexity is bound to increase when further ingredients are added to the curved spacetime environment where the test particles move. A typical instance of that is represented by the electromagnetic fields, the inclusion of which in the analysis of the curved spacetime dynamics of charged particles is interesting and important both theoretically and astrophysically.

In regard to this instance, application of the exact analytical solutions for the Maxwell's equations in a Schwarzschild or Kerr background determined in [7–14] has provided useful insight into the charged particle dynamics in the "magnetic field plus strong spacetime curvature scenario" [15–28]. The obvious difficulties such as the full three-dimensional analysis vs the restricted equatorial one, the nonseparability of the Hamilton-Jacobi equation for the nongeodesic case, the notably more complex equations of motion which have to be integrated and which do not allow an analytical solution anymore have so far suggested a softer approach to the nonequatorial problem. In fact, past work on the nonequatorial charged particle behavior in the external electromagnetic fields given by the above mentioned exact analytical solutions [7–14] has focused on the Schwarzschild case [15,17,23,24,27,28], while the Kerr analysis has been limited to equatorial motions [16,17,19–21,25] or quasiequatorial motions [18,22] only.

We now wish to make a step further in the nonequatorial analysis, with the rotation of the gravitational source taken into account. Employing the solution determined by Wald [9] for the uniform magnetic field in a Kerr background, in Sec. II we write the nongeodesic equations of motion for the full three-dimensional case explicitly. The identification of a physically sensible set of initial data for their numerical integration is the subject of Sec. III, while Sec. IV illustrates and comments on the characteristics of the trajectories thus obtained. A summary of the results and the conclusions of the paper are found in the final Sec. V.

Notation and conventions: we employ $G = 1 = c$ units throughout, with the exception of the final formulas, where the c factors are explicited and the places where the G factors are to be inserted are explicitly indicated as well, for the benefit of the reader. Apart from the specific Boyer-Lindquist coordinate indices $\{t, r, \vartheta, \varphi\}$, generic Greek indices are employed to identify four-dimensional ("spacetime") quantities, while generic Latin indices indicate the three-dimensional ("local three-space") ones. Overdots indicate derivatives with respect to the proper time τ: $\dot{x}^\alpha \equiv dx^\alpha/d\tau$, $\ddot{x}^\alpha \equiv d^2x^\alpha/d\tau^2$; $D/d\tau$ represents

*giovanni.preti@pd.infn.it

the absolute derivative with respect to τ; the four-velocity $u^\alpha \equiv \dot{x}^\alpha$ is normalized according to $u^\alpha u_\alpha = -1$ (metric signature $+2$); observers and observables are identified by their respective four-velocities; hatted indices refer to tetrad quantities; and a tilde superscript indicates that the corresponding quantity is a "per unit mass" term.

II. EQUATIONS OF MOTION

The Kerr metric in usual Boyer-Lindquist coordinates reads

$$ds^2 = -\left(1 - \frac{2Mr}{\Sigma}\right)dt^2 + \frac{\Sigma}{\Delta}dr^2 + \Sigma d\vartheta^2 + \frac{A}{\Sigma}\sin^2\vartheta d\varphi^2 - \frac{4aMr\sin^2\vartheta}{\Sigma}dtd\varphi, \quad (1)$$

where

$$\Sigma = r^2 + a^2\cos^2\vartheta, \quad (2)$$

$$\Delta = r^2 + a^2 - 2Mr, \quad (3)$$

$$A = (r^2 + a^2)^2 - a^2\Delta\sin^2\vartheta = (r^2 + a^2)\Sigma + 2Mra^2\sin^2\vartheta, \quad (4)$$

with M and a representing the mass and the specific angular momentum of the gravitational source (condition $a > 0$ is understood).

The field potential A_α of the Wald solution [9] to the Maxwell's equations in the Kerr background, corresponding to an asymptotically uniform magnetic field aligned along the symmetry axis, is given by

$$\begin{pmatrix} A_t \\ A_\varphi \end{pmatrix} = B_0 \begin{pmatrix} g_{tt} & g_{t\varphi} \\ g_{t\varphi} & g_{\varphi\varphi} \end{pmatrix} \begin{pmatrix} a \\ 1/2 \end{pmatrix}, \qquad A_r = 0 = A_\vartheta, \quad (5)$$

where B_0 is the asymptotic modulus of the magnetic field. From this field potential the following expression for the electromagnetic field $F_{\alpha\beta} = 2\partial_{[\alpha}A_{\beta]}$ is derived:

$$F_{\alpha\beta} = B_0\frac{aM}{\Sigma^2}\begin{pmatrix} 0 & f_{tr} & f_{t\vartheta} & 0 \\ -f_{tr} & 0 & 0 & f_{r\varphi} \\ -f_{t\vartheta} & 0 & 0 & f_{\vartheta\varphi} \\ 0 & -f_{r\varphi} & -f_{\vartheta\varphi} & 0 \end{pmatrix}, \quad (6)$$

where

$$f_{tr} = (r^2 - a^2\cos^2\vartheta)(1 + \cos^2\vartheta),$$
$$f_{t\vartheta} = r(r^2 - a^2)\sin 2\vartheta,$$
$$f_{r\varphi} = \left\{\frac{r\Sigma^2}{aM} + a(r^2 - a^2\cos^2\vartheta)(1 + \cos^2\vartheta)\right\}\sin^2\vartheta,$$
$$f_{\vartheta\varphi} = \left\{\frac{\Sigma^2}{2aM}(r^2 + a^2) - ar[2(r^2 + a^2)\cos^2\vartheta + a^2\sin^4\vartheta]\right\}\sin 2\vartheta.$$

Expression (6) can be inserted into the Lorentz equation:

$$\frac{D}{d\tau}u^\alpha = \tilde{q}F^\alpha{}_\beta u^\beta \quad (7)$$

to obtain the dynamics of a particle $\mathbf{u}$ of mass m and charge q (recall $\tilde{q} \equiv q/m$) in the presence of the given electromagnetic field. Because of the symmetries of the problem, the t and φ components of the momentum $p_\alpha = mu_\alpha + qA_\alpha$ are constants of the motion:

$$p_t = \text{const} \equiv -E, \qquad p_\varphi = \text{const} \equiv \ell, \quad (8)$$

neither of which is relative to the particle alone, due to the contributions coming from the field potential. In particular, E and ℓ do *not* identify the energy and azimuthal angular momentum of the particle with respect to a far-away observer, as it happens with the simpler geodesic case instead.

The presence of the magnetic field (6) does not allow the problem of determining the particle motion to be reducible to quadratures, since the Hamilton-Jacobi equation is not separable now, nor can recurse be made to an efficient potential for the analytical characterization of the orbits. A different path must therefore be followed: numerical integration of the trajectories has to be done, and a characterization of the charged particle behavior can be obtained by individuating and examining some significative examples, as we are going to see.

The dynamics of the charged particle is fully described by the set consisting of the two first-order equations for the variables t and φ obtained from (8), and of the two second-order equations for the variables r and ϑ obtained from (7). This set reads

$$\dot{t} = \frac{1}{\Delta\Sigma}\left\{A\left[\tilde{E} - \frac{1}{c}\tilde{q}B_0 a\left(1 - \frac{rM}{\Sigma}(2 - \sin^2\vartheta)\right)\right] - \frac{1}{c}2aMr\left[\tilde{\ell} - \frac{\tilde{q}B_0\sin^2\vartheta}{\Sigma}\left(\frac{A}{2} - 2Mra^2\right)\right]\right\}, \quad (9)$$

$$\ddot{r} + \frac{\Delta M}{\Sigma^3}(r^2 - a^2\cos^2\vartheta)(c\dot{t})^2 - \frac{2a\Delta M\sin^2\vartheta}{\Sigma^3}(r^2 - a^2\cos^2\vartheta)c\dot{t}\,\dot{\varphi} - \frac{1}{\Delta\Sigma}[(r^2 - a^2\cos^2\vartheta)M - ra^2\sin^2\vartheta]\dot{r}^2 - \frac{a^2\sin 2\vartheta}{\Sigma}\dot{r}\,\dot{\vartheta} - \frac{\Delta r}{\Sigma}\dot{\vartheta}^2 + \frac{\Delta\sin^2\vartheta}{\Sigma} \times \left[\frac{Ma^2\sin^2\vartheta}{\Sigma^2}(r^2 - a^2\cos^2\vartheta) - r\right]\dot{\varphi}^2 = \tilde{q}B_0\frac{a\Delta M}{\Sigma^3}\left\{-(r^2 - a^2\cos^2\vartheta)(1 + \cos^2\vartheta)c\dot{t} + \sin^2\vartheta\left[\frac{r\Sigma^2}{aM} + a(r^2 - a^2\cos^2\vartheta)(1 + \cos^2\vartheta)\right]\dot{\varphi}\right\}, \quad (10)$$

$$\ddot{\vartheta} - \frac{Mra^2\sin 2\vartheta}{\Sigma^3}(c\dot{t})^2 + \frac{2(r^2+a^2)Mra\sin 2\vartheta}{\Sigma^3}c\dot{t}\,\dot{\varphi} + \frac{a^2\sin 2\vartheta}{2\Sigma\Delta}\dot{r}^2 + \frac{2r}{\Sigma}\dot{r}\,\dot{\vartheta} - \frac{a^2\sin 2\vartheta}{2\Sigma}\dot{\vartheta}^2 - \frac{\sin 2\vartheta}{2\Sigma^3} \times [(r^2+a^2)\Sigma^2 + 2a^2Mr\sin^2\vartheta(2\Sigma + a^2\sin^2\vartheta)]\dot{\varphi}^2 = \tilde{q}B_0\frac{aM}{\Sigma^3}\left\{[-r(r^2-a^2)\sin 2\vartheta]c\dot{t} + \sin 2\vartheta\left[\frac{(r^2+a^2)\Sigma^2}{2aM} - ar(2(r^2+a^2)\cos^2\vartheta + a^2\sin^4\vartheta)\right]\dot{\varphi}\right\}, \tag{11}$$

$$\dot{\varphi} = \frac{1}{\Delta\Sigma}\left\{2aMr\left[c\tilde{E} - \tilde{q}B_0 a\left(1 - \frac{rM}{\Sigma}(2-\sin^2\vartheta)\right)\right] + \left(\frac{\Delta}{\sin^2\vartheta} - a^2\right)\left[\tilde{\ell} - \frac{\tilde{q}B_0\sin^2\vartheta}{\Sigma}\left(\frac{A}{2} - 2Mra^2\right)\right]\right\}, \tag{12}$$

where the dimensional c factors have been explicited, and the Kerr parameters M and a are expressed in units of length (hence, in the above equations it is intended that $M \to GM/c^2$ wherever it appears, explicitly or implicitly, and $a = \alpha M$, with $\alpha \in [0, 1]$). The set of equations (9)–(12) does not allow an analytical solution; it has to be solved numerically, once a consistent set of initial data and constants of motion is imposed. Discussion about this issue is the subject of the next section.

III. PHYSICAL MEASUREMENTS

Recalling $\tilde{E} \equiv E/m$ and $\tilde{\ell} \equiv \ell/m$, from Eqs. (8) we have:

$$\tilde{E} = -(g_{tt}\dot{t} + g_{t\varphi}\dot{\varphi} + \tilde{q}A_t), \tag{13}$$

$$\tilde{\ell} = g_{t\varphi}\dot{t} + g_{\varphi\varphi}\dot{\varphi} + \tilde{q}A_\varphi, \tag{14}$$

neither of which is a particle-related quantity alone, due to the contributions coming from field potential, as remarked above. This implies that, if we wish to keep direct control on the initial data relative to the *particle*, we cannot first fix the values of $\tilde{E}$ and $\tilde{\ell}$, and from these derive the former, but we must proceed the other way around, instead. The normalization condition $u^\alpha u_\alpha = -1$ for the particle four-velocity $u^\alpha = \{\dot{t}, \dot{r}, \dot{\vartheta}, \dot{\varphi}\}$ gives

$$\dot{t}_{\pm} = \frac{1}{-g_{tt}}[g_{t\varphi}\dot{\varphi} \pm \sqrt{g_{t\varphi}^2\dot{\varphi}^2 - g_{tt}(g_{rr}\dot{r}^2 + g_{\vartheta\vartheta}\dot{\vartheta}^2 + g_{\varphi\varphi}\dot{\varphi}^2 + 1)}], \tag{15}$$

from which we obtain, with c factors explicited,

$$\tilde{E}_{\pm} = \frac{1}{c}[\pm\sqrt{g_{t\varphi}^2\dot{\varphi}^2 - g_{tt}(g_{rr}\dot{r}^2 + g_{\vartheta\vartheta}\dot{\vartheta}^2 + g_{\varphi\varphi}\dot{\varphi}^2 + c^2)} - \tilde{q}A_t], \tag{16}$$

$$\tilde{\ell}_{\pm} = \frac{1}{-g_{tt}}[\Delta\sin^2\vartheta\dot{\varphi} \pm g_{t\varphi}\sqrt{g_{t\varphi}^2\dot{\varphi}^2 - g_{tt}(g_{rr}\dot{r}^2 + g_{\vartheta\vartheta}\dot{\vartheta}^2 + g_{\varphi\varphi}\dot{\varphi}^2 + c^2)}] + \tilde{q}A_\varphi. \tag{17}$$

The two couples of values thus found, $\{\tilde{E}_+, \tilde{\ell}_+\}$ and $\{\tilde{E}_-, \tilde{\ell}_-\}$, which the constants of motions (13) and (14) can take, can be expressed in terms of the initial data $\{r_0, \vartheta_0, \dot{r}_0, \dot{\vartheta}_0, \dot{\varphi}_0\}$. Choosing the former or the latter of these two couples is in general not arbitrary. In fact,

(i) the absence of chronology violation regions in the Kerr black hole spacetime ($a \leq M$) implies that the condition $\dot{t} > 0$ holds everywhere;

(ii) the existence of an ergosphere for the Kerr solution, in correspondence to $g_{tt} = 0$, implies that g_{tt} is negative outside the radius of the ergosphere:

$$r_{\rm erg}(\vartheta; M, a) = M + \sqrt{M^2 - a^2\cos^2\vartheta}, \tag{18}$$

and positive inside;

(iii) for a Kerr black hole spacetime the condition $g_{t\varphi} < 0$ always holds.

Hence, putting all these points together, it follows that, if $r > r_{\rm erg}$ then $\{\tilde{E}_+, \tilde{\ell}_+\}$ is the only allowed choice, while if $r < r_{\rm erg}$ both the $\{\tilde{E}_+, \tilde{\ell}_+\}$ and the $\{\tilde{E}_-, \tilde{\ell}_-\}$ couples are allowed.

In order to obtain physically realistic particle trajectories, the initial data characterizing the particle must obviously correspond to realistic physical quantities. Since the initial "velocity" data required for the integration of Eqs. (9)–(12), namely, the coordinate derivatives $\dot{r}_0$ and $\dot{\vartheta}_0$, do *not* represent components of the *physical* velocity of the particle, there is not an obvious physical criterion telling us how to choose the values for these coordinate derivatives so that the couple $\{\dot{r}_0, \dot{\vartheta}_0\}$ thus selected would actually correspond to a physically meaningful choice. To this end, we must *first* refer to a set of *physical measurements* for the components of the particle velocity, and *then* we must express $\dot{r}_0$ and $\dot{\vartheta}_0$ as a function of them. It therefore becomes now necessary to introduce an observer, located at the initial spacetime position of the particle, who can operate the above measurements.

Let us consider a (wholly generic) observer **k**, who wishes to make a physical measurement of the spatial velocity of the particle **u** [29]. To begin with, **k** has to assign a spatial velocity vector **v** to **u**. This is obtained by projecting the four-velocity **u** of the particle on the rest space of **k**, using the spatial projector $P(k)^\alpha{}_\beta = \delta^\alpha_\beta + k^\alpha k_\beta$, and then expressing the result in terms of **k**'s proper time. The components of **v** therefore read

$$v^\alpha \equiv -\frac{P(k)^\alpha{}_\beta u^\beta}{(u_\sigma k^\sigma)} = \frac{u^\alpha}{\tilde{\gamma}} - k^\alpha, \tag{19}$$

where

$$\tilde{\gamma} = -u_\alpha k^\alpha \tag{20}$$

is the energy of $\mathbf{u}$ as measured in the local rest frame of $\mathbf{k}$. The components (19) do not provide the components of the particle velocity as *physically measured* by the observer $\mathbf{k}$ yet. To obtain them, a tetrad projection is required:

$$v_{\hat{\imath}} = \lambda_{\hat{\imath}}{}^\alpha g_{\alpha\beta} v^\beta, \tag{21}$$

where the $\lambda_{\hat{\imath}}{}^\alpha$ are the components of the tetrad vectors of $\mathbf{k}$. The tetrad components (21) do finally provide us with the required physically meaningful quantities, namely, the measured components of the particle velocity. It is worth remarking that all of them—which obviously satisfy $v_{\hat{\imath}} \equiv v^{\hat{\imath}}$—have the correct dimensions of a velocity, namely LT^{-1}. This property is in general not shared by the contravariant components v^α defined in Eq. (19), instead, nor by their covariant counterparts v_α. It is also worth noting that the speed of $\mathbf{u}$ as physically measured by $\mathbf{k}$, namely $v = \sqrt{v_{\hat{\imath}} v^{\hat{\imath}}}$, can be obtained directly from (19) as $v = \sqrt{v_\alpha v^\alpha}$, since projection (21) does obviously not alter the modulus of $\mathbf{v}$. Thus, we immediately see that the locally measured energy (20) coincides with the locally measured Lorentz factor $\tilde{\gamma} = 1/\sqrt{1 - v^2}$.

Thus far, we have been dealing with an entirely *generic* observer $\mathbf{k}$; now, we specify this observer to be the Kerr zero-angular-momentum observer (ZAMO), whose four-velocity has components

$$k^\alpha = \frac{\delta^\alpha_t + \omega \delta^\alpha_\varphi}{\sqrt{-g_{tt} + \omega^2 g_{\varphi\varphi}}}$$

(where $\omega = -g_{t\varphi}/g_{\varphi\varphi}$ is the angular speed of inertial dragging), and whose tetrad frame is given by

$$\lambda_{\hat{t}} = \frac{\partial_t + \omega \partial_\varphi}{\sqrt{-g_{tt} + \omega^2 g_{\varphi\varphi}}}, \qquad \lambda_{\hat{r}} = \frac{\partial_r}{\sqrt{g_{rr}}},$$
$$\lambda_{\hat{\vartheta}} = \frac{\partial_\vartheta}{\sqrt{g_{\vartheta\vartheta}}}, \qquad \lambda_{\hat{\varphi}} = \frac{\partial_\varphi}{\sqrt{g_{\varphi\varphi}}}. \tag{22}$$

Equations (19) and (21) then allow expressing the proper time derivatives of the coordinates in terms of the physically meaningful particle velocity, as measured by the ZAMO, according to

$$\dot{r} = \tilde{\gamma} \frac{v_{\hat{r}}}{\sqrt{g_{rr}}}, \qquad \dot{\vartheta} = \tilde{\gamma} \frac{v_{\hat{\vartheta}}}{\sqrt{g_{\vartheta\vartheta}}},$$
$$\dot{\varphi} = \frac{\tilde{\gamma}}{\sqrt{g_{\varphi\varphi}}} \left(v_{\hat{\varphi}} - c \frac{g_{t\varphi}}{\sqrt{\Delta} \sin\vartheta} \right), \tag{23}$$

where the final expression follows from $v^\alpha k_\alpha \equiv 0$.

We have thus finally reached our aim; in fact, we are now in possession of all of the elements allowing us to proceed with an integration of the charged particle trajectories based on a physically meaningful choice for the initial data, established according to the following steps:

(i) First, we fix the initial spacetime location of the particle $\{t_0, r_0, \vartheta_0, \varphi_0\}$, with the obvious condition $r_0 > M + \sqrt{M^2 - a^2}$; note that the particular choice of both t_0 and φ_0 is not influential, due to the symmetries of the problem.

(ii) We fix the initial physical velocity of the particle, as measured by the colocated ZAMO $\{v_{\hat{r}0}, v_{\hat{\vartheta}0}, v_{\hat{\varphi}0}\}$, with the obvious condition $v_0 \equiv \sqrt{v^2_{\hat{r}0} + v^2_{\hat{\vartheta}0} + v^2_{\hat{\varphi}0}} < c$.

(iii) Then, from the set $\{r_0, \vartheta_0, v_{\hat{r}0}, v_{\hat{\vartheta}0}, v_{\hat{\varphi}0}\}$ fixed above, we obtain the coordinate derivatives $\{\dot{r}_0, \dot{\vartheta}_0, \dot{\varphi}_0\}$, by using Eqs. (23).

(iv) Then, from the set $\{r_0, \vartheta_0, \dot{r}_0, \dot{\vartheta}_0, \dot{\varphi}_0\}$ thus established, we derive the values (16) and (17) for the conserved quantities $\tilde{E}$ and $\tilde{\ell}$.

(v) Finally, the whole set $\{t_0, r_0, \vartheta_0, \varphi_0, \dot{r}_0, \dot{\vartheta}_0, \tilde{E}, \tilde{\ell}\}$ thus determined is employed in the numerical integration of the equations of motion (9)–(12).

Illustration and discussion of the resulting charged particle behavior is the subject of the next section.

IV. THE NONEQUATORIAL TRAJECTORIES

In order to deal with astrophysically realistic data, we assume the gravitational source to be represented by a supermassive galactic black hole of mass $M = 10^8 M_\odot$, and take for the magnetic field the value $B_0 = 10^{-13}$ T, which represents the estimated [30] upper limit for the strength of large scale homogeneous magnetic fields. As for the charged particles, we focus our analysis on electrons and positrons, since their charge-to-mass ratio, $\tilde{q} = \pm 1.78 \times 10^{11}$ C/kg, is the maximal one, thereby implying the maximal reactivity to the presence of the magnetic field.

The flat spacetime behavior of charged particles immersed in a uniform magnetic field along the z axis is quite simple, and well known; recall, in particular, that the axial freestreaming allows no possible charge confinement away from the equatorial plane (or from planes parallel to it, obviously). In a curved spacetime endowed with the corresponding Wald magnetic field (6), the situation changes remarkably. Already in the (relatively) simple case of a Schwarzschild background, the combination of the spacetime curvature with the external magnetic field can give rise to a complex structure of both cross-equatorial magnetically bottled orbits and axially collimated jet trajectories [28], suggestive of realistic astrophysical situations.

And if we add rotation to the source?

On the one hand, rotation is a matter of gravity, hence a *quantitative* modification of the Schwarzschild results is obviously expected. On the other hand, the gravitomagnetic field couples to the magnetic one in such a way as to remove the symmetries of the orbital motions with respect

to the sign of the particle charge [9], characterizing the Schwarzschild case; hence, we should also expect a remarkable *qualitative* change with respect to the latter.

Let us therefore begin to explore how a charged particle behaves in its nonequatorial motion around a Kerr black hole immersed in the Wald magnetic field.

Our initial approach is illustrated by Fig. 1, showing the evolution of the zenithal distance $\vartheta(\tau)$ of the charged particle, which is here an electron ejected radially (initial velocity $v_0 \equiv v_{\hat{r}0} = 0.9c$) from the surroundings of the black hole (initial position $r_0 = 6M$, $\vartheta_0 = 0.5$ rad); the extremal Kerr case is shown in comparison with the corresponding Schwarzschild and flat spacetime ones. The zenithal distance rapidly decreases, and the electron ultimately escapes in an axially collimated jetlike trajectory. The collimation effect, which is (obviously) already present in the flat spacetime case, becomes less rapid due to the gravitational attraction (as it is apparent from comparing between the Schwarzschild and the flat spacetime cases), but this attraction is counterbalanced and eventually overcome by the effects determined by the increasing rotation of the source (as the extremal Kerr case shows, in comparison with the other two).

A visualization of the trajectory of our electron is provided in Fig. 2, which shows the (x, z) section of its orbit in its early-time evolution (the time scale is one-fifth of that of Fig. 1). The axial collimation effect due to the magnetic field is made evident by the comparison with the trajectory (dashed line) which the electron would follow in the absence of the latter. It can also be observed that, although the flat (dotted line) and the extremal Kerr cases are qualitatively similar, quantitative differences do occur; in particular, enhanced escape velocity is observed in the latter case, as Fig. 1 already implied.

The effects of an increasing Kerr parameter can be appreciated in Fig. 3, which—in correspondence to the three values, $a = 0$ (Schwarzschild), $a = 0.5M$, and $a = M$ (extremal Kerr)—illustrates the early-time evolution of the above electron orbit [Fig. 3(a)], its ϑ evolution on a longer time scale [Fig. 3(b)], and the distance covered in the axial direction on a still longer time scale [Fig. 3(c)]. Again, it can be observed that the trajectories are qualitatively similar (jetlike escape, with no significant differences in the gyroradii), but in all three graphics there is an evident quantitative difference in the escape velocities, which confirms the role of an increasing Kerr parameter in favoring the ejection of our charged particle.

So far, we have dealt with an electron. What about positrons?

In a Schwarzschild background, we should not worry about the difference in the charge sign, since the electron/positron cases are specular (opposite $\tilde{q}$ + opposite $v_{\hat{\varphi}0} \rightarrow$ same behavior). But the gravitomagnetism which characterizes the Kerr case couples to the external magnetic field, causing a notable change in the charged particle behavior, depending on which of the two charges is considered. This

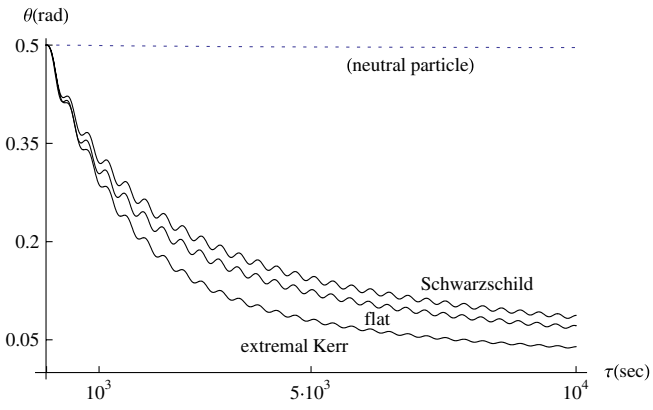

FIG. 1 (color online). Evolution of the zenithal distance ϑ for an initially radially ejected electron with $r_0 = 6M$, $v_{\hat{r}0} = 0.9c$, and $\vartheta_0 = 0.5$ rad, subject to the Wald field around an extremal ($a = M$) Kerr black hole, and comparison with the corresponding Schwarzschild and flat spacetime cases.

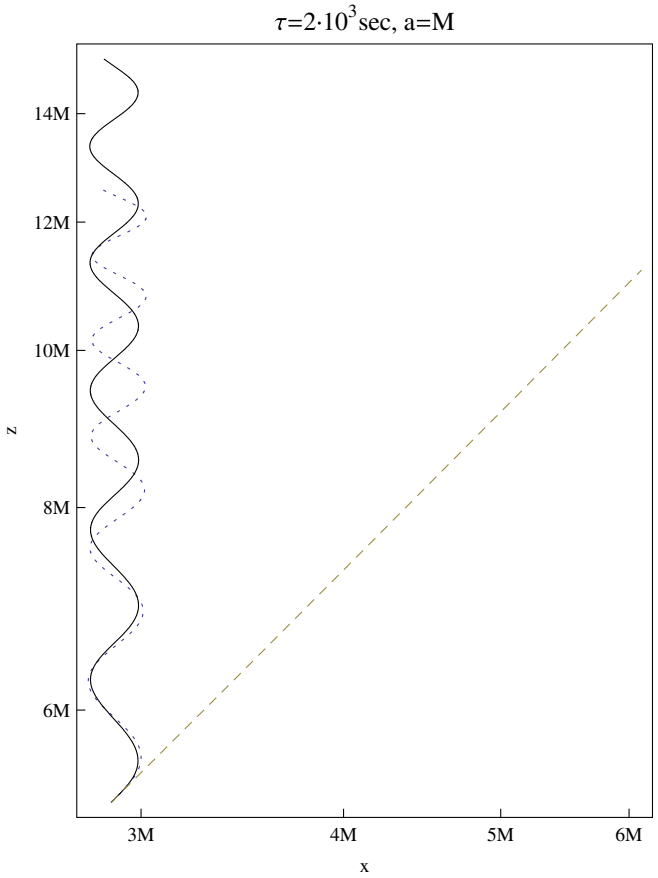

FIG. 2 (color online). (x, z) section of the orbit of an initially radially ejected electron (same initial data as in Fig. 1), moving in the Wald field around an extremal ($a = M$) Kerr black hole, compared with the trajectory in the corresponding "flat spacetime plus uniform magnetic field" case (dotted line), and with the behavior in the absence of the Wald field (dashed line).

change is not limited to quantitative differences in the same qualitative behavior, but also lets remarkable qualitative differences emerge. Both Figs. 4 and 5 refer to the same situation, namely, an electron or a positron with the *same* initial data in the *same* "Kerr + Wald magnetic field" environment, but the time scales are different: a shorter one for Fig. 4, and a longer one for Fig. 5. The former is already able to show the charge-dependent behavior of the two particles: with respect to the corresponding flat spacetime cases (dotted lines), axial acceleration is obtained for the electron, while the proton gets axially decelerated, instead. The trajectories are qualitatively similar, though, and this may naively lead one to think that the final outcome will be analogous to the one of Figs. 1–3, namely, a

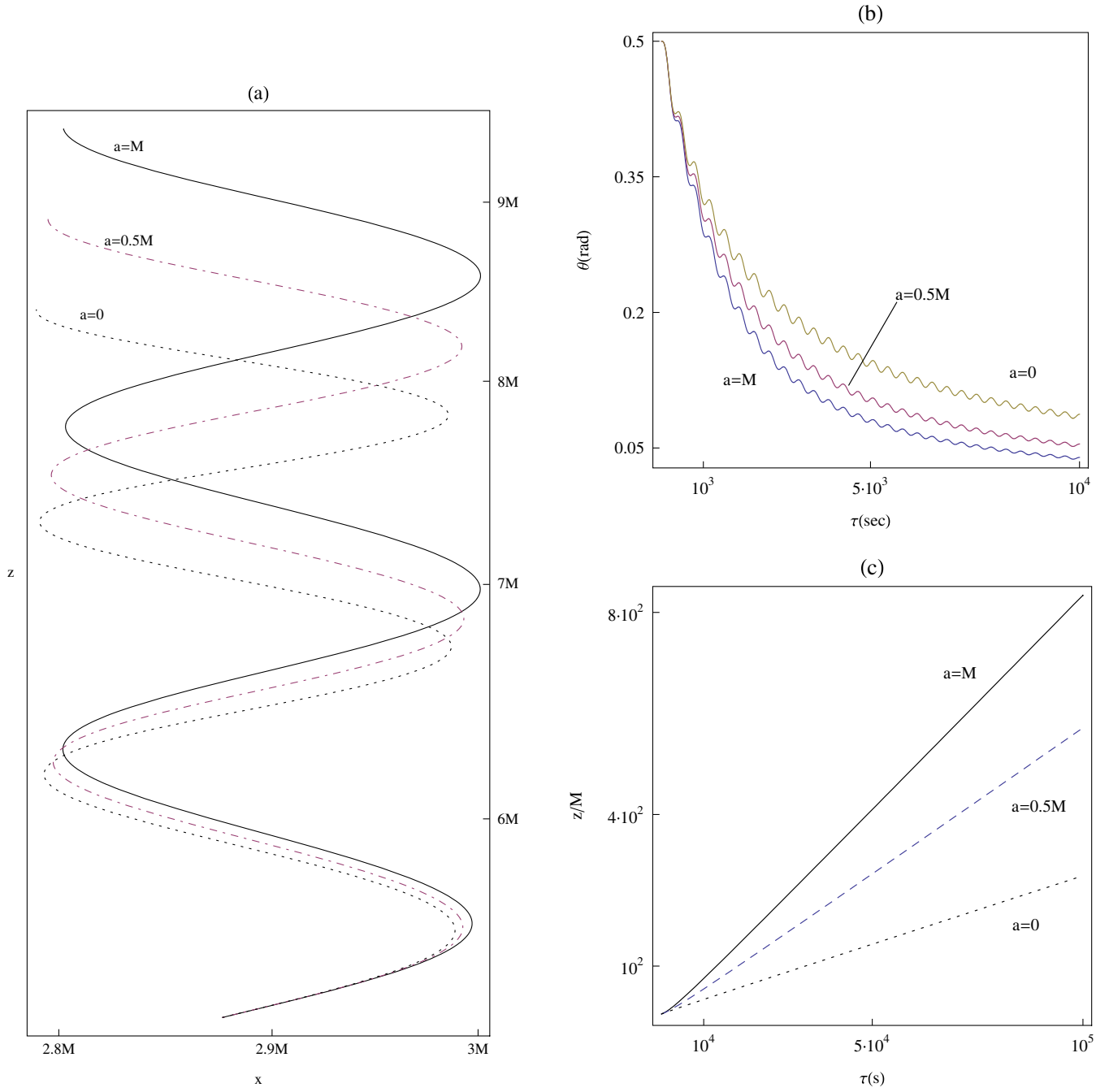

FIG. 3 (color online). (a) (x, z) section of the orbit of an initially radially ejected electron (same initial data as in Fig. 1) moving in the Wald field around a Kerr source, for different values of the Kerr parameter a (dotted line: Schwarzschild case; dashed line: $a = 0.5M$; solid line: extremal Kerr); plot for $0 \leq \tau \leq 10^3$ sec. (b) Evolution of the zenithal distance ϑ, for the three cases considered in (a). (c) Distance covered in the axial direction, for the three cases considered in (a).

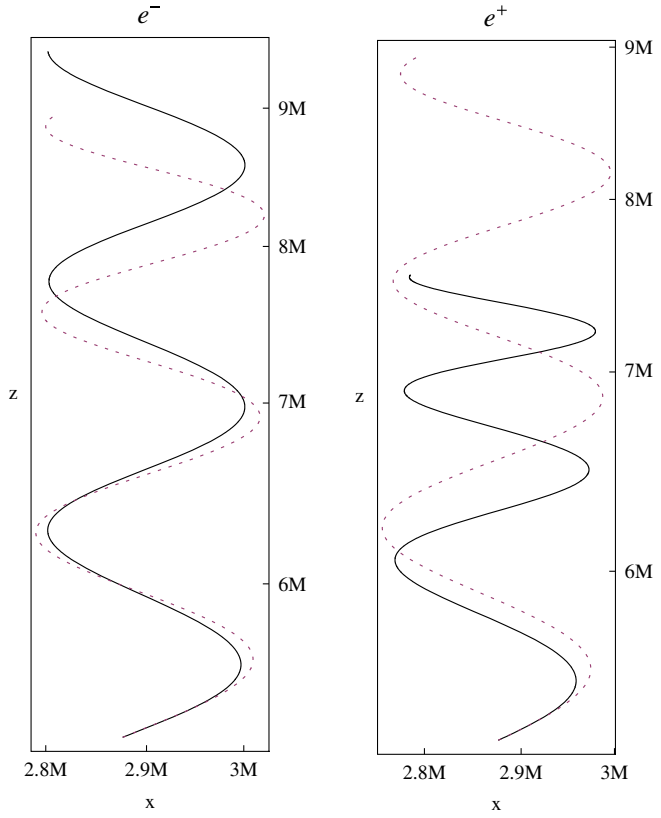

FIG. 4 (color online). (x, z) section of the orbit for an electron and a positron in the Wald field around an extremal Kerr black hole, and comparison with the corresponding flat spacetime case (dotted lines). Initial data as in Fig. 1; plots for $0 \leq \tau \leq 10^3$ sec .

jetlike escape, for both of the two cases. A look at the longer-time evolution of the trajectories will immediately correct such an impression. Indeed, as Fig. 5 clearly shows, the final outcome of the two trajectories is dramatically different: while the electron does succeed in its axially collimated escape away from the black hole, the positron gets magnetically entrapped in its surroundings instead, oscillating across the equatorial plane while precessing around the axis, *without* infalling into the horizon.

The above examples show that the combined effect of the magnetic and the gravitomagnetic fields can provide a natural mechanism for charge separation, selective charge confinement around the black hole, and selective charge ejection from the regions close to it. Do these particle behaviors crucially depend on the initial *direction* of the charged particle motion? In fact, we have so far been dealing with initially radially outgoing particles only; one might therefore reasonably think that an initial injection of the particles *toward* the black hole would rather easily prevent escape, instead, and easily lead to infall through the horizon as well. In order to see what happens when injection takes the place of ejection, we can invert the direction of the initial velocity $v_0 \equiv v_{\hat{r}0}$ while keeping all the other initial data unchanged with respect to the cases shown in Figs. 4 and 5. The results are illustrated in Figs. 6 and 7. The former shows the case of an initially radially infalling electron, which not only avoids being swallowed by the hole, but also does not even get so close to it as to trespass its ergosphere, as Fig. 6(b) shows. After a few rebounds back and forth in the magnetic field, our electron finally succeeds in escaping away, following an axially collimated jetlike trajectory in the negative-z direction, shown in Fig. 6(a). Figure 7 provides the correspondent of Fig. 6 (same initial data, same environment), but for the case of a positron. Again, the particle avoids being swallowed by the hole, and again it does not even cross its ergosphere [cf. Fig. 7(b)], but while the electron succeeded [cf. Fig. 6(a)], after a transient oscillatory phase, to escape the magnetogravitational trap, getting ultimately enrouted

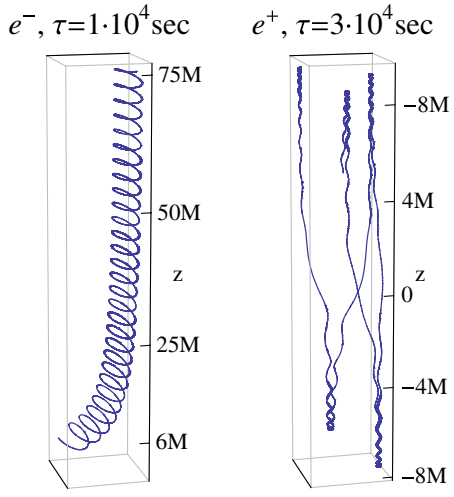

FIG. 5 (color online). 3D plots of the orbit for the electron and positron of Fig. 4.

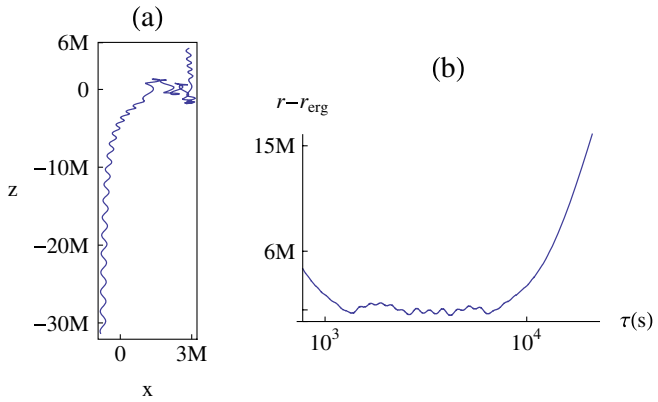

FIG. 6 (color online). Initially radially ingoing electron in the Wald field around an extremal Kerr black hole, with initial data $r_0 = 6M$, $v_{\hat{r}0} = -0.9c$, and $\vartheta_0 = 0.5$ rad. (a) (x, z) section of the orbit; (b) corresponding radial position of the particle with respect to the ergosphere. Time scales: $\tau_{\rm max} = 1.5 \times 10^4$ sec (a), $\tau_{\rm max} = 1.3 \times 10^4$ sec (b).

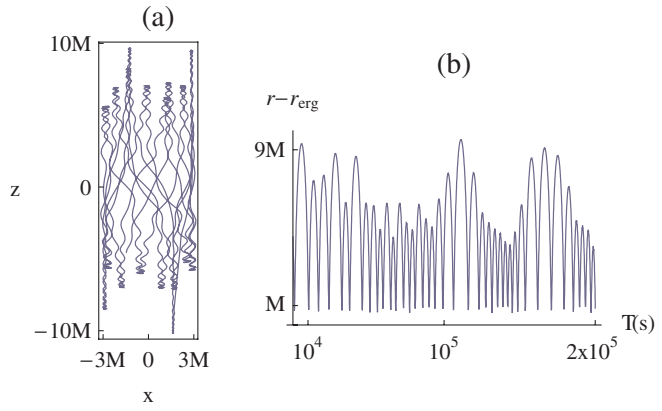

FIG. 7 (color online). As in Fig. 6, but for a positron. Time scales: $\tau_{\max} = 10^5$ sec (a), $\tau_{\max} = 2 \times 10^5$ sec (b).

into an axially collimated ejection, the positron gets entrapped around the hole [cf. Fig. 7(a)] instead, yet without—once again, as in the case of Fig. 5—infalling into it.

As remarked by Wald [9], a Kerr black hole in the uniform field (6) would, at variance with a Schwarzschild one, be subject to a selective charge accretion process from the surrounding ionized interstellar medium, leading the hole to evolve into a Kerr-Newman source. Although this evolution can be expected in general, the above examples have shown that an accreting charge is not *necessarily* doomed to infall across the horizon. In fact, the very magnetic interaction driving the selective accretion process is also able to confine the charge *around* the hole, preventing the latter from swallowing it, and thereby from building up electric charge itself. Thus, the neutrality of the Kerr source could be preserved, while a sort of ''ionosphere'' could form around it, where charges of the one sign are preferentially confined into, while the charges of the opposite sign can be efficiently pushed away from the regions close to the hole, along axially collimated jetlike trajectories.

These observations can be made more quantitative by evaluating the ''jetlike escape vs magnetic entrapment'' condition as a function of the initial velocities and of the initial zenithal distance characterizing our charged particles, in correspondence to various values of the Kerr parameter, in order to put into evidence the effects of the source rotation on the charged particle dynamics. The results of these evaluations are illustrated in Figs. 8 and 9.

In Fig. 8, the cases of initially radial ejections of both electrons (a) and positrons (b) are considered; for each given value of the Kerr parameter $\alpha \equiv a/M$, the boundary in the $\{v_{\hat{r}0}, \vartheta_0\}$ plane is shown which separates the escape trajectories (allowed *below* the corresponding α curves) from the magnetically confined ones (*above* them). As can easily be observed, at fixed initial data for the particle an increasing α favors the possibility of jetlike escape in the case of the electron [cf. Fig. 8(a)], while this possibility is hindered in the case of the positron [cf. Fig. 8(b)]. In

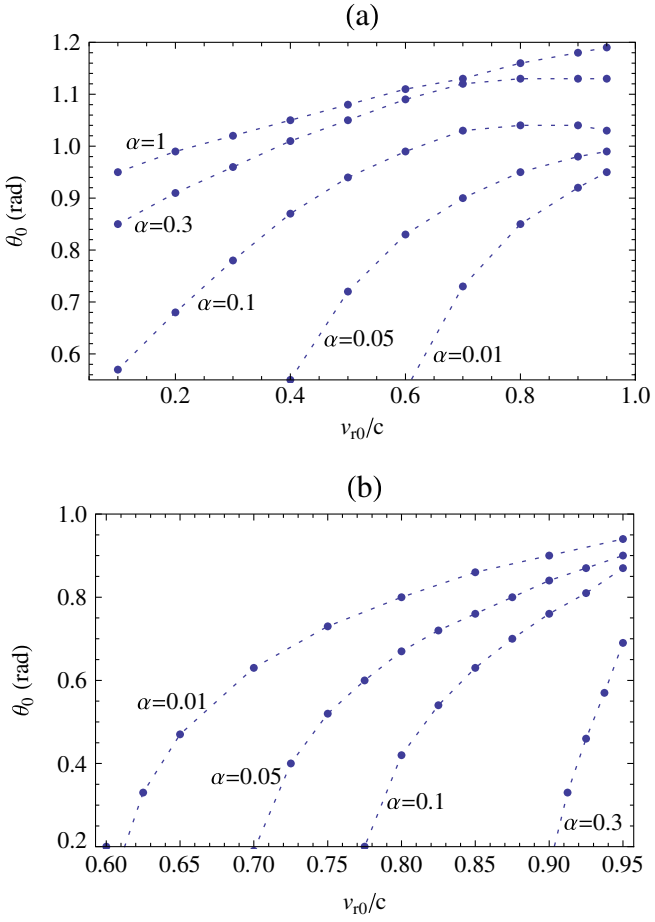

FIG. 8 (color online). Maximum escape initial zenithal distance ϑ_0 as a function of the initial velocity, for initially radial ejections of (a) electrons and (b) positrons, both starting from $r_0 = 6M$, in correspondence to different values of the parameter $\alpha = a/M$ (evaluations made with integration parameter $0 \leq \tau \leq 5 \times 10^5$ sec). Magnetically trapped orbits are found in correspondence to initial data within the region above each line, while escape trajectories (jetlike orbits) for values below.

particular, it is worth remarking that the whole of Fig. 8(b) actually fits in the lower-right corner of Fig. 8(a); this testifies the fact that in *any* case (with the obvious exception of the $\alpha = 0$ one) escape is always more problematic for positrons than for electrons, and much more so the more the rotation of the black hole increases. Thus, to the $(v_{\hat{r}0}, \vartheta_0)$ dependence of the magnetic confinement—characterizing *either* charge, cf. Figs. 8(a) and 8(b), and which could lead to the formation of a sort of ionosphere from whose open polar caps the more energetic particles of *either* charge can evade in axially collimated jetlike trajectories, in analogy to the Schwarzschild case [28]—here a rotation-induced effect is added, leading to a markedly charge-selective version of the same process: on equal initial terms, electrons ultimately dominate in the jet outcome, and positrons in the cross-equatorial magnetic trapping.

To complete the picture delineated by Fig. 8, we now shift our attention from the initially radial trajectories considered so far, with different initial zenithal distances, to the case of charged particles originally orbiting around the black hole in the equatorial plane, from which they are suddenly expelled by a vertical perturbation. This situation has a natural realistic counterpart in the orbital motions within accretion disks and in the powerful disk winds which can eject ionized particles at relativistic speed away from these same accretion disks. In correspondence to three representative values of the Kerr parameter ($a = 0.1M$, $a = 0.5M$, and $a = 1M$), Fig. 9 shows the region in the $(v_{\hat{\varphi}0}, v_{\hat{\vartheta}0})$ plane—bounded from above by the $v_0 = c$ curve—for initial data internal to which particle escape is found, both for the case of electrons (curves identified by the filled circles) and of positrons (curves with empty circles). The nonsymmetry of the curves with respect to $v_{\hat{\varphi}0} = 0$ is a consequence of the rotation of the black hole and of the presence of the Larmor gyromotion; more relevant for our analysis—and evident at a glance—is the fact that there is always less room for positrons to escape than for electrons: the latter are ejected more easily, while the former tend to get nonequatorially entrapped around the black hole. The separation of these behaviors is observed to become more pronounced the more the Kerr parameter increases, as a comparison of Fig. 9 from top to bottom clearly shows, in accord with our previous observations.

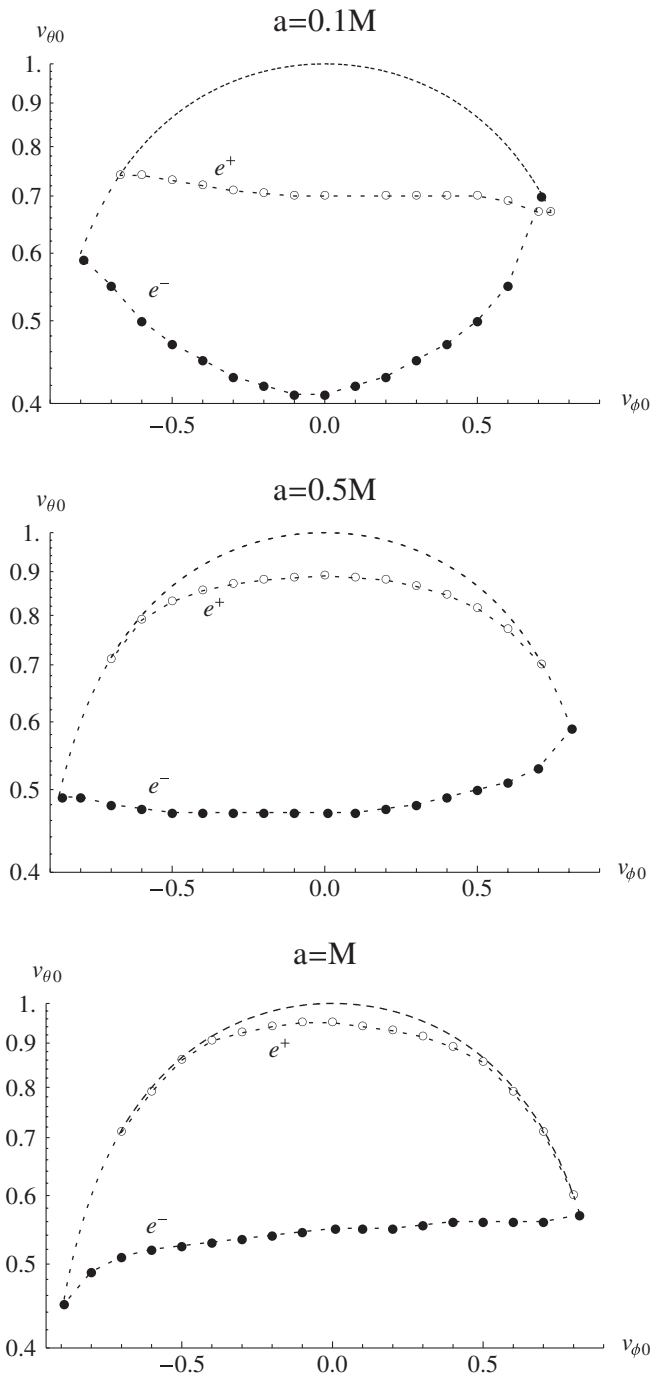

FIG. 9. Escape vs magnetic entrapment conditions, in terms of the initial angular velocities $v_{\hat{\varphi}0}$ and $v_{\hat{\vartheta}0}$, for electrons and positrons emerging from the equatorial plane, at $r_0 = 6M$ and with $v_{\hat{r}0} = 0$, in correspondence to different values of the Kerr parameter a (evaluations made with integration parameter $0 \leq \tau \leq 2 \times 10^5$ sec). Escape is obtained in correspondence to $\{v_{\hat{\varphi}0}, v_{\hat{\vartheta}0}\}$ couples inside the closed contour, bounded from above by the $v_0 = c$ curve, and from below by the curve with filled/empty circles (electron/positron cases, respectively).

Even if, for the reasons discussed in the Introduction and in Sec. II, an analytically detailed description of the orbits is not feasible for the problem we have been examining in this paper, the elements drawn from the illustrative cases presented above let us nonetheless outline a physically consistent picture of the relevant aspects which characterize the nonequatorial dynamics of our charged particles. It is now useful to summarize these aspects, drawing the conclusions from our analysis.

V. SUMMARY

The behavior of charged particles in electromagnetic fields when a strong spacetime curvature is present represents an interesting subject of enquiry, both from the purely theoretical and also from the astrophysical point of view. As such, it has been the subject of a series of papers [15–28], which have analyzed the charged particle dynamics around a Schwarzschild or a Kerr black hole immersed in the magnetic fields obtained in [7–14] as exact analytical solutions of the Maxwell's equations in the respective curved spacetime backgrounds. The studies for the Schwarzschild case have considered both equatorial and nonequatorial motions, but analysis of the charged particle dynamics around a Kerr source has been made for the restricted equatorial case [16,17,19–21,25] and the quasiequatorial case [18,22] only. This work has therefore aimed at providing an introductory extension to the full nonequatorial problem, by focusing on the nonequatorial trajecto-

ries of charged particles moving in the Wald magnetic field [9] around a Kerr black hole.

Use of Wald's exact solution allows the nongeodesic equations of motion to be written explicitly in the fully analytical form (9)–(12); however, their complexity does not allow analytical solutions: numerical ones must be sought, once a physically consistent set of initial data for the charged particle is individuated. Discussion of this issue has occupied Sec. III, while Sec. IV has provided a collection of illustrative examples which have progressively introduced us to the characterization of the charged particle dynamics, providing us with useful insight into the problem we wished to explore.

We have seen that the rotation of the source determines a marked difference between the behavior of the particles according to the sign of their charge, due to the coupling between the gravitomagnetism of the Kerr hole and the external magnetic field. In particular, we have seen that the charges of the one sign (the electrons, in our case) can more easily succeed in escaping away from the inner region, close to the hole, being efficiently boosted into axially collimated jetlike trajectories. The charges of the other sign (the positrons, in our case), on the contrary, are far more easily confined into cross-equatorial magnetically bottled orbits surrounding the Kerr black hole. The fact that such a ''confinement without infall'' is possible also shows that an accreting charge is not necessarily doomed to being swallowed by the hole, which in turn is therefore not necessarily doomed to evolve into a charged source.

The existence of such a mechanism for charge separation, able to lead both to selective charge confinement and to selective charge ejections, does represent not only an interesting subject of theoretical enquiry, but also an intriguing ingredient worth taking into account when the astrophysics of a rotating black hole immersed in a magnetic field and surrounded by ionized matter (see, e.g., [31]) is considered.

[1] B. Carter, Commun. Math. Phys. **10**, 280 (1968).
[2] M. Walker and R. Penrose, Commun. Math. Phys. **18**, 265 (1970).
[3] L. P. Hughston, R. Penrose, P. Sommers, and M. Walker, Commun. Math. Phys. **27**, 303 (1972).
[4] N. M. J. Woodhouse, Commun. Math. Phys. **44**, 9 (1975).
[5] B. Carter, Phys. Rev. D **16**, 3395 (1977).
[6] F. de Felice and G. Preti, Classical Quantum Gravity **16**, 2929 (1999).
[7] V. L. Ginzburg and L. M. Ozernoi, Zh. Eksp. Teor. Fiz. **47**, 1030 (1964) [Sov. Phys. JETP **20**, 689 (1965)].
[8] J. L. Anderson and J. M. Cohen, Astrophys. Space Sci. **9**, 146 (1970).
[9] R. M. Wald, Phys. Rev. D **10**, 1680 (1974).
[10] J. A. Petterson, Phys. Rev. D **10**, 3166 (1974).
[11] D. M. Chitre and C. V. Vishveshwara, Phys. Rev. D **12**, 1538 (1975).
[12] J. A. Petterson, Phys. Rev. D **12**, 2218 (1975).
[13] A. R. King, J. P. Lasota, and W. Kundt, Phys. Rev. D **12**, 3037 (1975).
[14] J. Bicak and L. Dvorak, Czech. J. Phys. B **27**, 127 (1977).
[15] A. R. Prasanna and R. K. Varma, Pramana **8**, 229 (1977).
[16] A. R. Prasanna and C. V. Vishveshwara, Pramana **11**, 359 (1978).
[17] A. R. Prasanna, Riv. Nuovo Cimento Soc. Ital. Fis. **3**, 1 (1980).
[18] A. N. Aliev and D. V. Gal'tsov, Gen. Relativ. Gravit. **13**, 899 (1981).
[19] A. R. Prasanna and N. Dadhich, Nuovo Cimento B **72**, 42 (1982).
[20] S. V. Dhurandhar and N. Dadhich, Phys. Rev. D **29**, 2712 (1984).
[21] S. V. Dhurandhar and N. Dadhich, Phys. Rev. D **30**, 1625 (1984).
[22] A. N. Aliev and D. V. Gal'tsov, Usp. Fiz. Nauk **157**, 129 (1989) [Sov. Phys. Usp. **32**, 75 (1989)].
[23] A. R. Prasanna and S. Sengupta, Phys. Lett. A **193**, 25 (1994).
[24] S. Sengupta, Int. J. Mod. Phys. D **6**, 591 (1997).
[25] A. N. Aliev and N. Özdemir, Mon. Not. R. Astron. Soc. **336**, 241 (2002).
[26] G. Preti, Classical Quantum Gravity **21**, 3433 (2004).
[27] J. Kovář, Z. Stuchlík, and V. Karas, Classical Quantum Gravity **25**, 095011 (2008).
[28] G. Preti, Int. J. Mod. Phys. D **18**, 529 (2009).
[29] F. de Felice and C. J. S. Clarke, *Relativity on Curved Manifolds* (Cambridge University Press, New York, 1990).
[30] J. D. Barrow, P. G. Ferreira, and J. Silk, Phys. Rev. Lett. **78**, 3610 (1997).
[31] J. H. Krolik, *Active Galactic Nuclei* (Princeton University Press, Princeton, NJ, 1998).